

Simulation of shear strain at arbitrary angles as a probe of packing instabilities

Chloe W. Lindeman* and Sidney R. Nagel

*Department of Physics and The James Franck and Enrico Fermi Institutes
The University of Chicago, Chicago, IL 60637, USA.*

(Dated: March 16, 2026)

Disordered solids distort and fail as particle contacts become unstable and rearrange under sufficiently large shear strains. Such instabilities can occur at different locations and, because of their proximity, can interact with one another. We develop a tool for simulations with periodic boundary conditions that allows strains to be applied at a continuously variable angle, θ . We show that instabilities can persist over a broad angular ranges of applied shear to form instability lines in phase space. By applying strain at different θ , we examine the correlations between the instabilities encountered at different angles and different positions in the sample. We find instabilities that pass through one another, others that change continuously as the angle is varied, and yet others that end by smoothly decreasing their magnitudes to zero as the instability fades away. Examining hysterons, *i.e.*, instabilities that undo themselves upon reversing the direction of shear, we find that as θ is varied towards the point where the instability disappears, the separation between the forward and backward instabilities shrinks to zero so as to produce an enhanced number of very small hysterons.

Solids deform when subjected to external stress. For sufficiently small stresses, the deformation is reversible and particles constituting the material return to their initial positions once the perturbation is removed. Under larger stress, the response can be catastrophic and irreversible. In disordered materials, *e.g.*, jammed packings or glasses, material failure can occur at numerous locations, known as soft spots, shear-transformation zones, or hysterons [1–4]. While there has been effort to predict where failure will occur [5, 6], there has been less focus on how the details of the forcing affect the response.

Previous simulations on jammed packings of soft spheres varied the angle of shear in free-standing packings with fixed boundaries [7–9]. Here we introduce a technique to apply shear strain in continuously variable directions in simulations with periodic boundary conditions. This allows investigation of bulk material away from any surfaces. It is readily applied in different dimensions, d , to systems of different sizes, N , and in dynamic or quasistatic scenarios. Using this technique, we map out instabilities encountered as a jammed packing of soft particles is sheared along different orientations. We then explore how different instabilities interact and how a single instability disappears as the shear angle is varied – features that would not be measurable using a fixed strain orientation.

Formalism for applying shear in arbitrary directions: It is intuitive to apply shear at an arbitrary angle for a two-dimensional system with a circular boundary: extend the system along one chosen axis and compress in the orthogonal direction [7–9]. Periodic boundary conditions, however, are more problematic because they require that the box shape be a parallelogram and that the particles that interact with those just inside one surface

should be a replica of the properly translated and shifted particles from the opposite boundary. Here we derive the required transformation for such a deformation.

In systems in d -dimensions with periodic boundaries we define the unit cell in terms of d lattice vectors and require the periodically continued copies to be offset from the original cell by integer multiples of those vectors. Varying the lattice vectors distorts the box and also shifts the neighboring cells so that they tile space smoothly as in Fig. 1a for $d = 2$. The problem then reduces to defining the appropriate shape of a box that corresponds to pure (p) or simple (s) shear at an arbitrary angle, θ .

In two dimensions, pure shear corresponds to extension along the positive diagonal, defined as $\theta = 0^\circ$, and compression in the orthogonal direction while simple shear corresponds to tilting the cell as in Fig. 1b,c respectively:

$$\Gamma_p(0) = \frac{1}{\sqrt{1 - \frac{\gamma_p^2}{4}}} \begin{bmatrix} 1 & \frac{\gamma_p}{2} \\ \frac{\gamma_p}{2} & 1 \end{bmatrix}; \quad \Gamma_s(0) = \begin{bmatrix} 1 & 0 \\ \gamma_s & 1 \end{bmatrix}$$

In these matrices, each column corresponds to one of the lattice vectors defining the sheared cell. The prefactor for pure shear ensures that cell volume remains constant. $\Gamma_s(0)$ corresponds to Lees-Edwards boundary conditions along the horizontal ($\theta = 0$) axis [10]. The desired transformations can be derived geometrically but it is simpler just to conjugate by a rotation matrix of arbitrary angle,

$$R_\theta = \begin{bmatrix} \cos \theta & -\sin \theta \\ \sin \theta & \cos \theta \end{bmatrix},$$

to find $\Gamma(\theta) = R_\theta \Gamma(0) R_\theta^{-1}$. This rotated transformation acting an arbitrary vector \vec{v} is therefore equivalent to rotating the vector by $-\theta$ ($R_\theta^{-1} \vec{v}$), applying the original transformation ($\Gamma(0) R_\theta^{-1} \vec{v}$) and then rotating back ($R_\theta \Gamma(0) R_\theta^{-1} \vec{v}$). For pure and simple strain, this leads to:

* cwindeman@jhu.edu

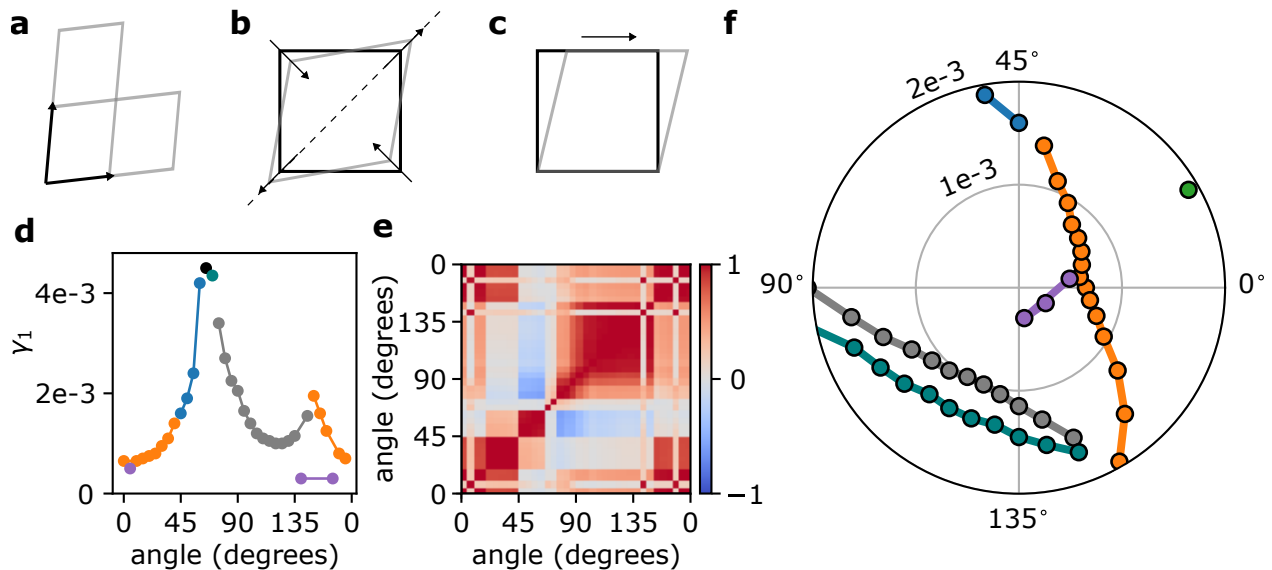


FIG. 1. (a) Definition of lattice vectors in $d = 2$, which define box shape and corresponding periodicity. (b) Pure and (c) simple shear along the chosen $\theta = 0^\circ$ for each case. For simple shear this corresponds to Lees-Edwards boundary conditions [10]. (d) Strain $\gamma_1(\theta)$ at which the first rearrangement event is encountered when shear is imposed along different directions θ ($N = 1021$, $d = 2$, $\Phi = 0.87$). (e) Normalized correlation $C(\theta_1, \theta_2)$ between particle motions of instabilities encountered upon shear in different directions θ_1 and θ_2 , with red indicating a high level of correlation and blue indicating negative correlation. (f) The same data as shown in (d) plotted in polar coordinates; color of data points indicates groupings determined from (e) with a threshold of $C > 0.9$. All rearrangements out to $\gamma = 0.002$ are included.

$$\Gamma_p(\theta) = \frac{1}{\sqrt{1 - \frac{1}{4}\gamma_p^2}} \begin{bmatrix} 1 - \frac{\gamma_p}{2} \sin(2\theta) & \frac{\gamma_p}{2} \cos(2\theta) \\ \frac{\gamma_p}{2} \cos(2\theta) & 1 + \frac{\gamma_p}{2} \sin(2\theta) \end{bmatrix} \quad (1)$$

consistent with [11] and

$$\Gamma_s(\theta) = \begin{bmatrix} 1 - \frac{\gamma_s}{2} \sin(2\theta) & -\frac{\gamma_s}{2} [1 - \cos(2\theta)] \\ \frac{\gamma_s}{2} [1 + \cos(2\theta)] & 1 + \frac{\gamma_s}{2} \sin(2\theta) \end{bmatrix}. \quad (2)$$

Note only 2θ appears, ensuring $\Gamma_{p,s}(\theta) = \Gamma_{p,s}(\theta + 180^\circ)$.

Simulations: We investigate the instabilities in particulate solids by applying shear at different angles to jammed packings of soft discs (in $d = 2$) and spheres (in $d = 3$) using the transformation for pure shear in Eq. (1) and its three-dimensional equivalent in the Appendix. Particles interact via the repulsive Hertzian potential:

$$V(r_{ij}) = \epsilon(1 - r_{ij}/\sigma_{ij})^{5/2}\Theta(\sigma_{ij} - r_{ij})$$

where ϵ sets the energy scale, ij label particles separated by distance r_{ij} , $\sigma_{ij} \equiv \sigma_i + \sigma_j$ is the sum of particle radii, and $\Theta(x)$ is the Heaviside function so that only overlapping particles interact. Radii are chosen from a log-normal distribution with polydispersity $P = 0.2$ in $d = 2$ and $P = 0.02$ in $d = 3$. The particle number, N , and packing fraction, Φ , are stated for each example.

Initial configurations are generated with random particle positions and quenched using the Fast Inertial Relaxation Engine (FIRE). For each deformation angle

measured, we begin with the same initial configuration and apply athermal quasistatic shear along a chosen shear direction θ using the pyCudaPacking software package [12, 13]. We choose small strain steps, between 5×10^{-5} and 5×10^{-3} , and test for rearrangements via reversibility as in [4]: we shear forward one strain step and minimize, then shear back and minimize, comparing the total energy of the packing before and after. This provides an unambiguous metric for determining whether an irreversible rearrangement has occurred.

Multiple instabilities in a given direction: At each angle, θ , one can start from the initial configuration and incrementally increase the strain until a first instability is reached. At that point the particles relax to new mechanically stable positions. One can continue increasing the strain beyond that point along the same angle to observe subsequent instabilities. $\gamma_\alpha(\theta)$ labels the strain at which the α^{th} instability occurs at angle θ . Figure 1(d) shows an example of $\gamma_1(\theta)$ for a two-dimensional packing of $N = 1021$ particles. In some angular regions, *e.g.*, $70^\circ < \theta < 140^\circ$, γ_α varies smoothly while elsewhere it abruptly jumps or changes slope.

Correlation of instabilities: For each rearrangement α , we record the displacement of all particles, $\Delta \vec{r}_\alpha$, which is an Nd -dimensional vector. In order to compare rearrangements that occur at different shear angles and magnitudes, the displacements $\Delta \vec{r}$ are first mapped back to the unit square cell by the inverse of the lattice vector matrix: $\Delta \vec{r}_0 = \Gamma^{-1} \Delta \vec{r}$. Following [8, 9], we then use

these displacements to compare rearrangements α and β that occur at angles θ_1 and θ_2 by calculating the normalized correlation,

$$C_{\alpha,\beta}(\theta_1, \theta_2) = \frac{\sum_{i=1}^{Nd} \Delta \vec{r}_{0,\alpha}(\theta_1) \cdot \Delta \vec{r}_{0,\beta}(\theta_2)}{|\Delta \vec{r}_{0,\alpha}(\theta_1)| |\Delta \vec{r}_{0,\beta}(\theta_2)|}.$$

Figure 1(e) shows the correlation between the first rearrangements at all angles, θ , as a matrix where the color of row θ_i and column θ_j indicates the magnitude of C for those instabilities. Red represents high correlation so that large blocks of red on the diagonal reveal rearrangements that persist across that range of angles. The colors in Fig. 1(d,f) are assigned so that rearrangements with $C > 0.9$ have the same color. (This is an associative process, so that if two rearrangements A and B are correlated, and B and C are correlated, then A and C are also grouped together.) The smooth regions in Fig. 1(d) suggest an instability that persists over a range of θ and a discontinuity reveals a change in the instability, as generally confirmed by the coloration.

Polar plots: The structure of the instability is perhaps more clearly appreciated by plotting $\gamma_\alpha(\theta)$ in polar coordinates as in Fig. 1(f). The radial direction indicates the strain magnitude, $|\gamma|$, while the azimuthal direction indicates the axis of extension θ . Note that θ varies only from 0 to 180° (instead of 360°) so that the periodicity in 2θ is explicitly manifested. By again grouping rearrangements with correlation $C > 0.9$, we see that continuous regions generally correspond to instabilities that persist over a range of angles. Other examples showing the strains where rearrangements occur for a range of sizes, $7 \leq N \leq 1021$, and in both $d = 2$ and $d = 3$ are shown in Fig. 4 of the Appendix.

When replotted in polar coordinates as in Fig. 1(b), the characteristic curved features seen in Fig. 1(a) in Cartesian coordinates become much straighter. Though imperfect, these segments suggest a geometric interpretation: the soft spot being triggered has an inherent 0° – 180° symmetry, and the relevant information is not the total strain γ but rather the projection of the strain matrix onto the orientation of this feature. Given that rearrangements are often expected to take the form of quadrupolar displacements [14–16], this may not be so surprising. However, the real-space images of the rearrangements often bear little resemblance to a quadrupole, as in Fig. 2(b), yet the characteristic shape of $\gamma_1(\theta)$ persists even at the smallest system sizes. This suggests that a geometric signature of failure events may still exist even when a coarse-grained approach is not possible.

Features of instability lines: One striking feature, also found in systems with fixed boundaries [7–9], is that a single rearrangement can persist over an extended angular region, sometimes greater than 90°. Because of the 180° periodicity, deformations that are 90° apart correspond to shear in opposite directions. This is at odds with a naive picture of shear where one would expect that opposite deformations lead to entirely different responses, as in force chains with an orientation determined by the

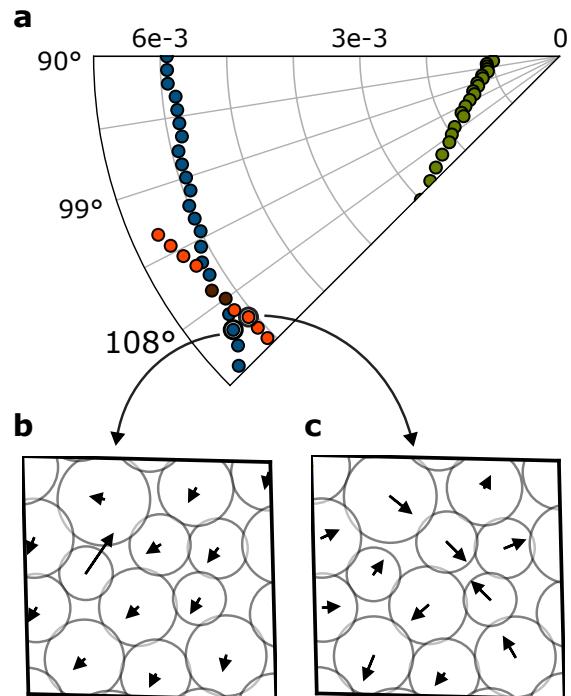


FIG. 2. (a) Part of a polar plot showing an example of two rearrangement lines ($C = 0.076$ when comparing the circled rearrangements) that cross ($N = 13$, $d = 2$, $\Phi = 0.9$). The finite step size causes the rearrangements to occur in the same strain step for two of the angles tested; this is not well-correlated with either the blue or red rearrangement individually (hence its distinct color) but is very well correlated ($C = 0.99$) with the *sum* of the two crossing rearrangements. (b,c) Real space image of rearrangement events highlighted in (a) with arrows indicating the direction and relative magnitudes of displacements.

direction of shear. Unless both instability endpoints extend past the chosen 0° and 180° directions, performing forward and backward shear along only one axis would entirely miss the existence of such large persistence.

Figure 1(f) shows not only the first rearrangement for each deformation angle but also subsequent instabilities at the same angle. By tracking the correlations of all rearrangements found, it is possible to study the behavior of two rearrangements as they approach one another. Figure 2(a) shows one observed behavior: two lines of rearrangements cross. Because the system is small, the two rearrangements cannot spatially avoid one another, yet Fig. 2(b,c) show that the particle displacements are quite different for the two rearrangements, allowing them to pass through one another with minimal interaction.

Along with crossing instability lines, one can examine how rearrangement lines end. We illustrate several possibilities using the example in Fig. 1(e,f). In some cases, one rearrangement line runs into another and vanishes as seen where the purple rearrangement hits the orange. In other cases, one rearrangement transitions

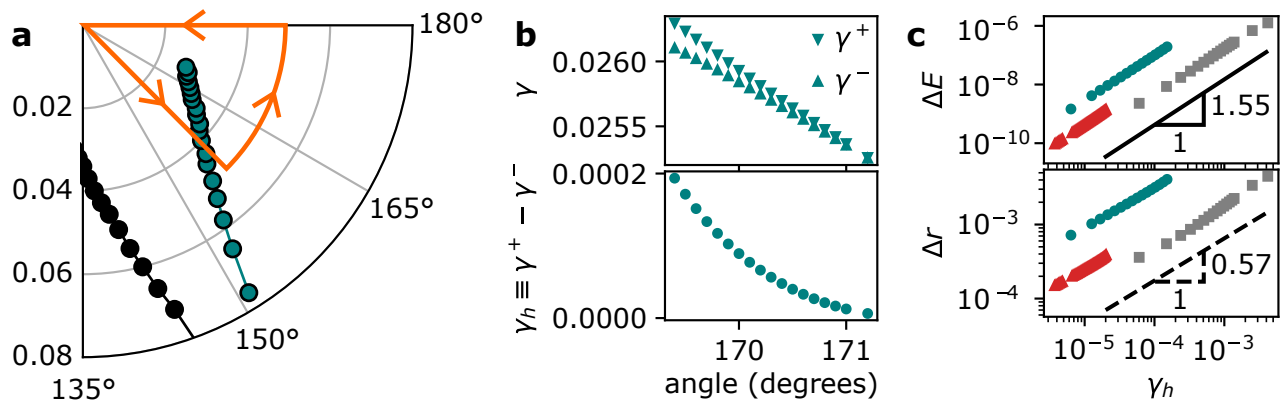


FIG. 3. (a) An example ($N = 11$, $d = 2$, $\Phi = 0.9$) of a rearrangement that appears to end abruptly (teal rearrangement, end occurs around $\theta = 170^\circ$). The orange path shows a trajectory that starts at the origin, goes radially outward crossing the teal line of rearrangements, azimuthally to $\theta = 180^\circ$, and then returns to the origin. (b) Strain values of rearrangements encountered in both directions γ^+ and γ^- (top) and the difference between them γ_h (bottom) versus angle. (c) Energy drop, ΔE , (top) and particle displacements, Δr , (bottom) versus hysteresis γ_h for each point shown in (b) (teal circles) as well as the equivalents for two other hysterons measured (grey squares: $N = 11$, $\Phi = 0.9$; red triangles: $N = 17$, $\Phi = 0.87$). Average of the three best-fit exponents are shown as guides to the eye (ΔE : 1.55 ± 0.04 ; Δr : 0.57 ± 0.05).

gradually to another as indicated by a gradual variation of the color in the correlation matrix, for example between $\theta = 80^\circ$ and $\theta = 100^\circ$. In yet other cases, a rearrangement line changes abruptly from one rearrangement to another without a large jump in strain as in the transition from orange to blue around 45° . The abrupt nature of such a transition is revealed only in the correlation matrix by a sudden change in color (here, the transition from dark to light red at $\theta = 45^\circ$). Finally, a rearrangement line may end abruptly without another rearrangement nearby. We examine this last case below.

Closing of hysterons: We can modify the loading protocol to study the behavior of instabilities that belong to the class of rearrangements called *hysterons*: as the strain is increased a rearrangement is encountered at a strain γ^+ but when the system is sheared back to the original box shape along the same path (that is, radially inward) the rearrangement is undone via a second rearrangement at $\gamma^- < \gamma^+$ so the system reverts to its original configuration. Hysterons have played an important role [17–24] in trying to understand the memories that can be stored in cyclically sheared solids [2–4, 25–30].

We show here that a line of such paired rearrangements can end via vanishing hysteresis: $\gamma_h \equiv \gamma^+ - \gamma^- \rightarrow 0$ as the shear angle θ reaches the end of rearrangement line. This is the case for the teal rearrangement in Fig. 3(a) as θ increases as plotted in Fig. 3(b). Note that the result is a rearrangement line that appears to end abruptly, as is also seen in Figs. 1(f) and 2(a). Because the hysteresis values measured quickly become small, once rearrangements are found using a fixed step size of 10^{-5} or 2×10^{-5} , we localize rearrangements to within 10^{-9} of the actual strain values γ^+ and γ^- using a bisection algorithm before reporting hysteresis and measuring the energy drop ΔE and the norm of the particle displacements

$\Delta r \equiv \sqrt{\Delta \vec{r} \cdot \Delta \vec{r}}$.

As shown in Fig. 3(c), the energy drop ΔE and particle displacements Δr associated with each rearrangement also decrease smoothly with γ_h as the hysteron ends; both quantities scale with γ_h with exponent consistent with 1.5 for ΔE and 0.6 for Δr . This is true both for the hysteron shown in Fig. 3(a) (teal circles) and for two other hysterons examined in detail (grey squares: $N = 11$, $\Phi = 0.9$; red triangles: $N = 17$, $\Phi = 0.87$). A similar, but much more noisy, relationship has been seen in an ensemble of packings (*i.e.*, different configurations), each measured at a single angle $\theta = 0$ [4]. The ability to vary the shear angle continuously reveals that scaling behavior is intrinsic to individual rearrangements, with variability (in the form of different coefficients to the power law) from rearrangement to rearrangement. Far from the endpoints, the behavior of the hysteresis, energy drop, and displacements deviates from the smooth behavior substantially; we have therefore focused on the consistent behavior observed close to the end of each hysteron.

Circumventing an instability: Finally, we modify the path through phase space to avoid an instability entirely by going around the rearrangement line. As an example, we measured rearrangements along a path radially outward through the rearrangement line, azimuthally around to 180° , and back to the origin as shown in orange in Fig. 3(a). This circuitous return path circumvents the teal rearrangement line examined above. Indeed, the only rearrangement detected is that moving outward as we pass through the teal line, yet the packing returns its initial configuration upon returning to zero strain. Thus, one may reach identical particle configurations via not only different paths, but via paths both with and without rearrangements.

Future directions: We have demonstrated how to sim-

ulate systems with periodic boundary conditions while shear is applied at an arbitrary angle. This allowed us to probe features of failure events in jammed packings that could not be observed using traditional Lees-Edwards boundary conditions [10] (uni-axial simple shear) or uni-axial pure shear. For example, it revealed that rearrangement lines sometimes cross through one another, other times merge into a single rearrangement, or simply end as the instability magnitude drops continuously to zero. This work also opens the door to other studies of amorphous solids. By collecting rearrangement statistics, we can study correlations between rearrangement persistence and the size of the resulting energy basins to better understand how materials form memories of the applied deformation. In addition, the technique can be extended to network solids, suspensions and even to fluids.

ACKNOWLEDGEMENTS

We thank Eric Corwin, Spencer Fajardo, Michael Falk, Carl Goodrich, Varda Hagh, Peter Y. Lu, Joshua Mundinger, Muhittin Mungan, Itamar Proccacia, and

Damien Vandembroucq for insightful conversations. This work was supported by the US Department of Energy, Office of Science, Basic Energy Sciences, under Grant DE-SC0020972. Computational resources were provided by the NSF MRSEC program NSF-DMR 2011854.

APPENDIX: VARYING SIZE AND DIMENSIONALITY

In some cases, rearrangements can persist for a range of shear angles exceeding 90° . To illustrate the ubiquity of this behavior, Fig. 4a-c shows additional examples across system sizes: $7 \leq N \leq 1021$.

In $d = 3$, there are five independent shear types and hence many ways to choose two independent axes for a polar plot. Figure 4d shows a $d = 3$ example where we have applied pure shear strain in the $X - Y$ plane:

$$\Gamma_p(\theta) = \begin{bmatrix} \frac{1}{\sqrt{1-\frac{1}{4}\gamma_p^2}} \left[\begin{array}{cc} 1 - \frac{\gamma_p}{2} \sin(2\theta) & \frac{\gamma_p}{2} \cos(2\theta) \\ \frac{\gamma_p}{2} \cos(2\theta) & 1 + \frac{\gamma_p}{2} \sin(2\theta) \end{array} \right] & 0 \\ 0 & 1 \end{bmatrix}$$

-
- [1] M. L. Falk and J. S. Langer, Dynamics of viscoplastic deformation in amorphous solids, *Physical Review E* **57**, 7192 (1998).
 - [2] N. C. Keim and P. E. Arratia, Yielding and microstructure in a 2d jammed material under shear deformation, *Soft Matter* **9**, 6222 (2013).
 - [3] N. C. Keim and P. E. Arratia, Mechanical and microscopic properties of the reversible plastic regime in a 2d jammed material, *Physical review letters* **112**, 028302 (2014).
 - [4] C. W. Lindeman and S. R. Nagel, Minimal cyclic behavior in sheared amorphous solids, *New Journal of Physics* **27**, 085001 (2025).
 - [5] D. Richard, M. Ozawa, S. Patinet, E. Stanifer, B. Shang, S. Ridout, B. Xu, G. Zhang, P. Morse, J.-L. Barrat, *et al.*, Predicting plasticity in disordered solids from structural indicators, *Physical Review Materials* **4**, 113609 (2020).
 - [6] S. A. Ridout, J. W. Rocks, and A. J. Liu, Correlation of plastic events with local structure in jammed packings across spatial dimensions, *Proceedings of the National Academy of Sciences* **119**, e2119006119 (2022).
 - [7] O. Gendelman, P. K. Jaiswal, I. Procaccia, B. S. Gupta, and J. Zylberg, Shear transformation zones: State determined or protocol dependent?, *Europhysics Letters* **109**, 16002 (2015).
 - [8] S. Patinet, D. Vandembroucq, and M. L. Falk, Connecting local yield stresses with plastic activity in amorphous solids, *Physical Review Letters* **117**, 045501 (2016).
 - [9] M. Lerbinger, *Local shear rearrangements in glassy systems: from micromechanics to structural relaxation in supercooled liquids*, Ph.D. thesis, Université Paris sciences et lettres (2020).
 - [10] A. W. Lees and S. F. Edwards, The computer study of transport processes under extreme conditions, *Journal of Physics C: Solid State Physics* **5**, 1921 (1972).
 - [11] C. W. Lindeman, Multi-dimensional memory in low-friction granular materials, *Soft Matter* **21**, 4890 (2025).
 - [12] P. K. Morse and E. I. Corwin, Geometric signatures of jamming in the mechanical vacuum, *Physical Review Letters* **112**, 115701 (2014).
 - [13] P. Charbonneau, E. I. Corwin, G. Parisi, and F. Zamponi, Jamming criticality revealed by removing localized buckling excitations, *Physical Review Letters* **114**, 125504 (2015).
 - [14] J. D. Eshelby, The determination of the elastic field of an ellipsoidal inclusion, and related problems, *Proceedings of the royal society of London. Series A. Mathematical and physical sciences* **241**, 376 (1957).
 - [15] V. Chikkadi, G. Wegdam, D. Bonn, B. Nienhuis, and P. Schall, Long-range strain correlations in sheared colloidal glasses, *Physical review letters* **107**, 198303 (2011).
 - [16] C. Maloney and A. Lemaitre, Subextensive scaling in the athermal, quasistatic limit of amorphous matter in plastic shear flow, *Physical review letters* **93**, 016001 (2004).
 - [17] F. Preisach, Über die magnetische nachwirkung, *Zeitschrift für physik* **94**, 277 (1935).
 - [18] J. P. Sethna, K. Dahmen, S. Kartha, J. A. Krumhansl, B. W. Roberts, and J. D. Shore, Hysteresis and hierarchies: Dynamics of disorder-driven first-order phase transformations, *Phys. Rev. Lett.* **70**, 3347 (1993).
 - [19] M. Mungan, S. Sastry, K. Dahmen, and I. Regev, Networks and hierarchies: How amorphous materials learn to remember, *Phys. Rev. Lett.* **123**, 178002 (2019).
 - [20] N. C. Keim, J. Hass, B. Kroger, and D. Wieker, Global memory from local hysteresis in an amorphous solid, *Phys. Rev. Research* **2**, 012004 (2020).
 - [21] M. M. Terzi and M. Mungan, State transition graph of the preisach model and the role of return-point memory, *Physical Review E* **102**, 012122 (2020).

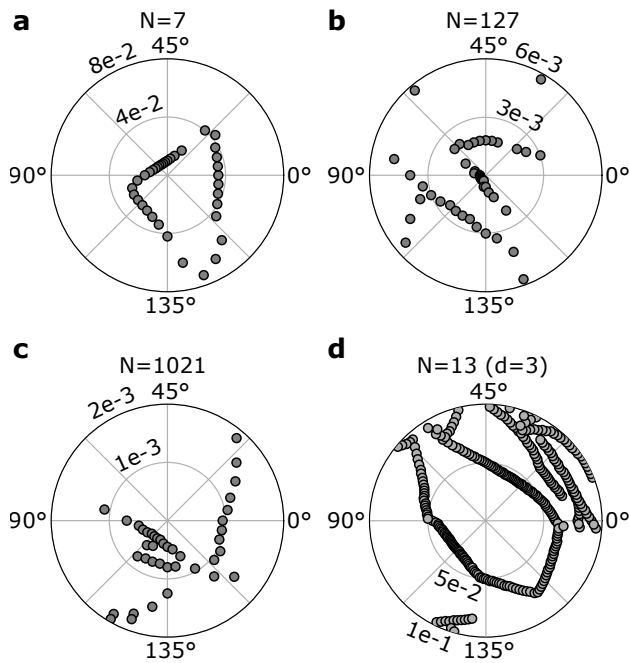


FIG. 4. Lines of instabilities for various system sizes: (a) $N = 7$, (b) $N = 127$, and (c) $N = 1021$ for $d = 2$, $\Phi = 0.87$, and polydispersity $P = 0.2$. (d) Similar behavior is found in three dimensions with $N = 13$, $d = 3$, $\Phi = 0.75$ and $P = 0.02$.

- [22] M. van Hecke, Profusion of transition pathways for interacting hysterons, *Physical Review E* **104**, 054608 (2021).
- [23] A. Szulc, M. Mungan, and I. Regev, Cooperative effects driving the multi-periodic dynamics of cyclically sheared amorphous solids, *The Journal of Chemical Physics* **156** (2022).
- [24] D. Shohat, D. Hexner, and Y. Lahini, Memory from coupled instabilities in unfolded crumpled sheets, *Proceedings of the National Academy of Sciences* **119**, e2200028119 (2022).
- [25] I. Regev, T. Lookman, and C. Reichhardt, Onset of irreversibility and chaos in amorphous solids under periodic shear, *Phys. Rev. E* **88**, 062401 (2013).
- [26] D. Fiocco, G. Foffi, and S. Sastry, Oscillatory athermal quasistatic deformation of a model glass, *Physical Review E—Statistical, Nonlinear, and Soft Matter Physics* **88**, 020301 (2013).
- [27] N. Perchikov and E. Bouchbinder, Variable-amplitude oscillatory shear response of amorphous materials, *Physical Review E* **89**, 062307 (2014).
- [28] D. Fiocco, G. Foffi, and S. Sastry, Encoding of memory in sheared amorphous solids, *Physical review letters* **112**, 025702 (2014).
- [29] J. R. Royer and P. M. Chaikin, Precisely cyclic sand: Self-organization of periodically sheared frictional grains., *Proc. Natl. Acad. Sci.* **112**, 49 (2015).
- [30] M. O. Lavrentovich, A. J. Liu, and S. R. Nagel, Period proliferation in periodic states in cyclically sheared jammed solids, *Phys. Rev. E* **96**, 020101 (2017).